



# M3 Wave System Modeling

## Cooperative Research and Development Final Report

**CRADA Number: CRD-17-697**

NREL Technical Contact: Yi-Hsiang Yu

**NREL is a national laboratory of the U.S. Department of Energy  
Office of Energy Efficiency & Renewable Energy  
Operated by the Alliance for Sustainable Energy, LLC**

This report is available at no cost from the National Renewable Energy Laboratory (NREL) at [www.nrel.gov/publications](http://www.nrel.gov/publications).

Contract No. DE-AC36-08GO28308

**Technical Report**  
NREL/TP 5000-75410  
November 2019



# M3 Wave System Modeling

## Cooperative Research and Development Final Report

**CRADA Number: CRD-17-697**

NREL Technical Contact: Yi-Hsiang Yu

### **Suggested Citation**

Yu, Yi-Hsiang. 2019 *M3 Wave System Modeling: Cooperative Research and Development Final Report, CRADA Number CRD-17-697*. Golden, CO: National Renewable Energy Laboratory. NREL/TP-5000-75410. <https://www.nrel.gov/docs/fy20osti/75410.pdf>.

**NREL is a national laboratory of the U.S. Department of Energy  
Office of Energy Efficiency & Renewable Energy  
Operated by the Alliance for Sustainable Energy, LLC**

This report is available at no cost from the National Renewable Energy Laboratory (NREL) at [www.nrel.gov/publications](http://www.nrel.gov/publications).

Contract No. DE-AC36-08GO28308

**Technical Report**  
NREL/TP 5000-75410  
November 2019

National Renewable Energy Laboratory  
15013 Denver West Parkway  
Golden, CO 80401  
303-275-3000 • [www.nrel.gov](http://www.nrel.gov)

## NOTICE

This work was authored by the National Renewable Energy Laboratory, operated by Alliance for Sustainable Energy, LLC, for the U.S. Department of Energy (DOE) under Contract No. DE-AC36-08GO28308. Funding provided by U.S. Department of Energy Office of Energy Efficiency and Renewable Energy Wind and Water Technologies Office and U.S. Department of Energy Small Business Voucher Program. The views expressed herein do not necessarily represent the views of the DOE or the U.S. Government.

This work was prepared as an account of work sponsored by an agency of the United States Government. Neither the United States Government nor any agency thereof, nor any of their employees, nor any of their contractors, subcontractors or their employees, makes any warranty, express or implied, or assumes any legal liability or responsibility for the accuracy, completeness, or any third party's use or the results of such use of any information, apparatus, product, or process disclosed, or represents that its use would not infringe privately owned rights. Reference herein to any specific commercial product, process, or service by trade name, trademark, manufacturer, or otherwise, does not necessarily constitute or imply its endorsement, recommendation, or favoring by the United States Government or any agency thereof or its contractors or subcontractors. The views and opinions of authors expressed herein do not necessarily state or reflect those of the United States Government or any agency thereof, its contractors or subcontractors.

This report is available at no cost from the National Renewable Energy Laboratory (NREL) at [www.nrel.gov/publications](http://www.nrel.gov/publications).

U.S. Department of Energy (DOE) reports produced after 1991 and a growing number of pre-1991 documents are available free via [www.OSTI.gov](http://www.OSTI.gov).

*Cover Photos by Dennis Schroeder: (clockwise, left to right) NREL 51934, NREL 45897, NREL 42160, NREL 45891, NREL 48097, NREL 46526.*

NREL prints on paper that contains recycled content.

**Cooperative Research and Development Final Report**

**Report Date: March 8, 2019**

In accordance with requirements set forth in the terms of the CRADA agreement, this document is the final CRADA report, including a list of subject inventions, to be forwarded to the DOE Office of Science and Technical Information as part of the commitment to the public to demonstrate results of federally funded research.

**Parties to the Agreement:** M3 Wave, LLC

**CRADA number:** CRD-17-697

**CRADA Title:** M3 Wave System Modeling

**Joint Work Statement Funding Table showing DOE commitment:**

<b>Estimated Costs</b>	<b>NREL Shared Resources a/k/a Government In-Kind</b>
Year 1	\$ 100,000.00
TOTALS	\$ 100,000.00

**Abstract of CRADA Work:**

M3 Wave is a leader in submerged pressure differential wave energy harvesting technology. M3 Wave’s approach to developing technology is focused on simplicity and survivability. The company has been working on wave energy devices since 1991 and has produced a number of successes during that time. During testing as part of DOE’s Wave Prize finals, M3 Wave encountered an unexpected phenomenon that increased power production by over 25% in their NEXUS system. The problem to be explored by this project is how to accurately model and characterize this phenomenon to better take advantage of the potential benefits. This will be accomplished by: 1) developing and validating a system-hydrodynamics model of M3 Wave’s NEXUS system; 2) performing a parameter study to identify possible mechanisms for improved energy capture, and 3) providing M3 Wave with a working, adaptable, model of their system, such that M3 Wave is able to incorporate the study’s findings and optimize their system for improved LCOE.

**Summary of Research Results:**

The purpose of the SBV project is to further investigate this unexpected behavior. M3 Wave devices could be able to improve Annual Energy Production (AEP) and reduce capital cost, thereby improving Levelized Cost of Energy (LCOE). NREL is supporting M3 on technology development, focusing on hydrodynamics modeling and assisting design exploration and exploiting the unexpected phenomenon that increased power production by over 25% in their NEXUS system during the Wave Energy Prize wave tank test. The project includes three tasks. Here are a brief description of the research conducted for each task:

- Task I - Develop the System-Hydrodynamics Model: A frequency-domain system hydrodynamics model of M3 Wave’s 1:50 scale NEXUS WEC was created based on the device information and properties provided by M3. NREL used the model to simulate the experimentally observed device dynamics, including heave, surge, sway, pitch, yaw, and roll motions. This was accomplished utilizing generalized body modes to model the additional degrees of freedom introduced by the dynamic mooring system, including articulated joints, bending, tension/compression, and torsion modes, as required to capture the physics of interest.
- Task II - Identify Mechanisms for Improved Energy Capture : Followed by the effort to explore and identify the system-hydrodynamic mechanisms by which energy capture may potentially be improved and provide device parameter suggestions to M3 Wave to incorporate these phenomena.
- Task III: Dissemination: The description of research conducted in this project is documented in the attached summary report and the conference paper.

Results can be found in the report entitled “M3 SBV Project Summary Report” and “Numerical Analysis and Validation of a Pressure-Differential Wave Energy Converter” conference paper below.

**Subject Inventions Listing:**

None

**ROI #:**

None

**Responsible Technical Contact at Alliance/NREL:**

Yi-Hsiang Yu, [Yi-Hsiang.Yu@nrel.gov](mailto:Yi-Hsiang.Yu@nrel.gov)

**Name and Email Address of POC at Company:**

Mike Morrow, [mike@m3wave.com](mailto:mike@m3wave.com)

**DOE Program Office:**

Small Business Voucher (SBV) Program

# M3 SBV Project Summary Report

Fabian Wendt and Yi-Hsiang Yu

National Renewable Energy Laboratory

2019-03-08

## Introduction

M3 Wave is developing a unique submerged pressure differential wave energy conversion (WEC) device called DMP (Delos-Reyes Morrow Pressure). The DMP turns pressure fluctuations under ocean waves and swells into alternating expansion and compression cycles of an air-filled bladder. Two of these bladders are strategically oriented so they exchange air back and forth with each passing wave. This air exchange is harnessed using a bi-directional airturbine. The DMP concept has been incorporated into a stationary version on the ocean floor in shallow water (APEX) and a mid-column version tethered in deep water (NEXUS). APEX was tested in the open ocean in 2014 and NEXUS was a finalist for the Wave Energy Prize. Both versions operate below the ocean surface, avoiding extreme surface dynamics and conflicts with other ocean users common with floating systems.

As part of extensive wave tank testing at scales ranging from 1:50 up to 1:6 as well as 1:5 scale open water testing, M3 Wave has amassed a significant repository of characterization and performance data for the DMP. In particular, during Wave Energy Prize testing at 1:50 scale at the University of Michigan's wave tank, M3 Wave tested a variant of the NEXUS technology. It was essentially a DMP mated to a Tension Leg Platform (TLP) style of mooring. The expectation was that the dynamics would potentially rob efficiency from the system- however, the reverse turned out to be true. The TLP variant, which was free to gyrate, pitch, yaw, and roll under various wave conditions, experienced a 25% power increase over the static moored variant. It is unknown if this was a result of added hydrodynamic forces during roll events or if pitching added extra pressure differential or if something entirely unknown was contributing. This is a small business vouchers (SBV) project awarded to M3 Energy.

The purpose of the SBV project is to further investigate this unexpected behavior. M3 Wave devices could be able to improve Annual Energy Production (AEP) and reduce capital cost, thereby improving Levelized Cost of Energy (LCOE). NREL is supporting M3 on technology development, focusing on hydrodynamics modeling and assisting design exploration and exploiting the unexpected phenomenon that increased power production by over 25% in their NEXUS system during the Wave Energy Prize wave tank test. A frequency-domain system hydrodynamics model of M3 Wave's 1:50 scale NEXUS WEC is created based on the device information and properties provided by M3. NREL used the model to simulate the experimentally observed device dynamics, including heave, surge, sway, pitch, yaw, and roll motions. This was accomplished utilizing generalized body modes to model the additional degrees of freedom introduced by the dynamic mooring system, including articulated joints, bending, tension/compression, and torsion modes, as required to capture the physics of interest. Followed by the effort to explore and identify the system-hydrodynamic mechanisms by which energy capture may potentially be improved and provide device parameter suggestions to M3 Wave to incorporate these phenomena.

## Numerical Analysis and Validation Study

### *Numerical Model*

A numerical model was developed to simulate the taut moored M3 device for regular wave conditions. The numerical model is solved in the time domain to account for quadratic damping components, and the bag displacement is modeled as a piston type motion (Fig. 1). The utilized equations of motion are based on the work presented in Babarit et al. 2017, but additional degrees of freedom have been introduced to account for the motion of the device in its moored configuration. The equations of motion used in the numerical model are outlined below. They are formulated at the center of gravity which is located at the geometric center of the device (see Fig 1).

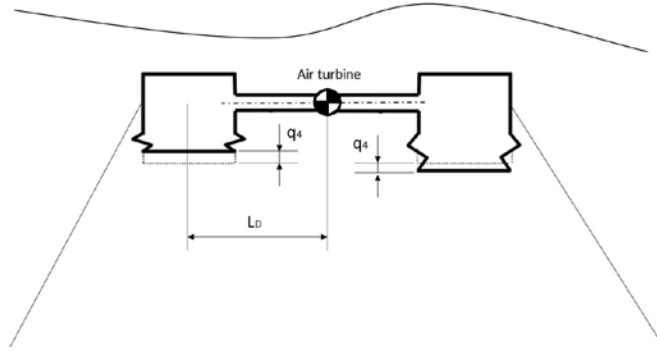


Figure 1. A taut moored M3 device with a piston-type bag mode shape. Graphic based on Babarit et al. 2017.

$$\mathbf{A}\ddot{\mathbf{q}} + \mathbf{B}\dot{\mathbf{q}} + \mathbf{D}\mathbf{v} + 0.5\mathbf{S}(\mathbf{p}_1 + \mathbf{p}_2) + (\mathbf{K} + \mathbf{C})\mathbf{q} = \mathbf{F}_{ex} \quad (1)$$

$$\dot{p}_1 - 0.5 \frac{\rho_s}{v_s} \mathbf{R}\dot{\mathbf{q}} + \frac{\rho_s}{v_s} \frac{p_1}{B_{PTO}} - \frac{\rho_s}{v_s} \frac{p_2}{B_{PTO}} = 0 \quad (2)$$

$$\dot{p}_2 + 0.5 \frac{\rho_s}{v_s} \mathbf{R}\dot{\mathbf{q}} - \frac{\rho_s}{v_s} \frac{p_1}{B_{PTO}} + \frac{\rho_s}{v_s} \frac{p_2}{B_{PTO}} = 0 \quad (3)$$

The matrix  $\mathbf{S}$  is only populated along the main diagonal and describes the relevant surface area that is participating in the coupled motion response between the rigid body modes and bag motion.  $\mathbf{R}$  contains the same entries as the diagonal of the  $\mathbf{S}$  matrix, arranged in a single row, and describes how the bag deforms as a result of coupled motion. The  $\mathbf{p}_1$  and  $\mathbf{p}_2$  vectors are simply populated with the  $p_1$  and  $p_2$  values:  $\mathbf{p}_{1_i} = p_1$  and  $\mathbf{p}_{2_i} = p_2$  for  $i = 1$  to 4. The  $\mathbf{A}$  matrix contains mass and inertia contributions from the device itself and from added mass effects.  $\mathbf{B}$  is the linear radiation damping matrix. The  $\mathbf{K}$  matrix represents the linear restoring contribution from the mooring system and the  $\mathbf{C}$  matrix contains the hydrostatic stiffness terms. More details of the numerical model were described in the study presented by Wendt, Yu, and Delos-reyes 2018.

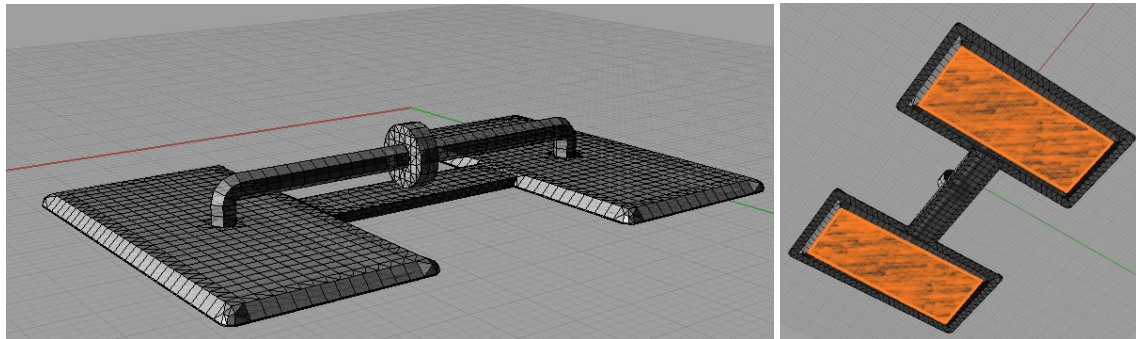


Figure 2. (Right) top isometric view of the WAMIT mesh; (left) bottom isometric view of the WAMIT mesh, where the bag surface participating in the piston mode shape is highlighted in orange.



**Figure 3. (Right) Marine Hydrodynamics Laboratory tow tank and carriage; (left) scaled M3 device installed in the tow tank (Steven 2016).**

The linear damping, added mass, and wave-excitation loads ( $F_{ex}$ ) caused by Froude-Krylov and scattering forces were computed via WAMIT Inc. 2016. An illustration of the utilized WAMIT mesh is shown in Fig. 2. The bag area that is participating in the piston motion is highlighted in orange. Quadratic damping resulting from viscous effects is included in the equation of motion through the  $\mathbf{D}$  matrix. A value of 8.0 was assigned to the viscous drag coefficient. Drag coefficients in the range between 8 and 10 are oftentimes used to model viscous effects in heave plates for offshore structures (Wendt et al. 2016; Wendt et al. 2015).

The salt water density, ( $1025 \text{ kg/m}^3$ ), is given as  $\rho$ , while  $\rho$  describes the density of the working fluid inside the wave energy device (in this case, air with  $1.225 \text{ kg/m}^3$ ). The equations of motion can be formulated as a system of differential equations and solved numerically.

#### **Wave Tank Testing**

A 1:50-scale version of the taut moored M3 device has been tested in the tow tank of the Marine Hydrodynamics Laboratory at the University of Michigan for the Wave Energy Prize in January 2016 (Steven 2016). The goal of the tests was the experimental characterization of the system's power performance over a range of different wave conditions. The M3 device used a turbine in the middle of the tube that connects the two flexible chambers to generate electrical power. For the model-scale test, the turbine was modeled through a simple orifice plate. The plate geometry was selected so that it produces a pressure drop similar to what would be expected from a model-scale turbine. Photos of the tow tank and the M3 device installed in the tow tank are shown in Fig. 3, respectively.

During the test, the generated power was computed from the measured pressure drop over the orifice plate. The exact procedure that was used to transfer the pressure measurements into an estimate of the generated power was not available to the authors. The device motions were recorded through an optical measurement system. The exact position relative to the device center that was used to report these motions was not known to the authors. Because of the large uncertainties associated with the recorded time series data, the authors focused their validation efforts on the motion amplitude and average power production data that were reported in table format for each test case.

#### **Comparison of Fixed versus Floating System**

To characterize the dynamic response of the numerical model, we computed the response amplitude operators (RAOs) and the averaged power production over a large range of different regular wave periods. Comparing a fixed versus a moored/floating configuration was one important aspect of our analysis. In the numerical model, the fixed configuration was realized by removing all coupling terms from the equations of motion. This approach yields a system of equations in which each degree of freedom is solved independently and the power performance and bag motion will not be impacted by the motion of the device (which basically represents a fixed system). Comparing the coupled and uncoupled numerical model makes it possible to quantify the impact of the device motion on the power performance of the system. All results presented and discussed in this paper are referring to the full scale version of the system. The length from chamber to device center ( $L_D$  in Fig. 1) for the full scale system is 25.0 m. The bottom of the device is submerged 12 m below the free surface.

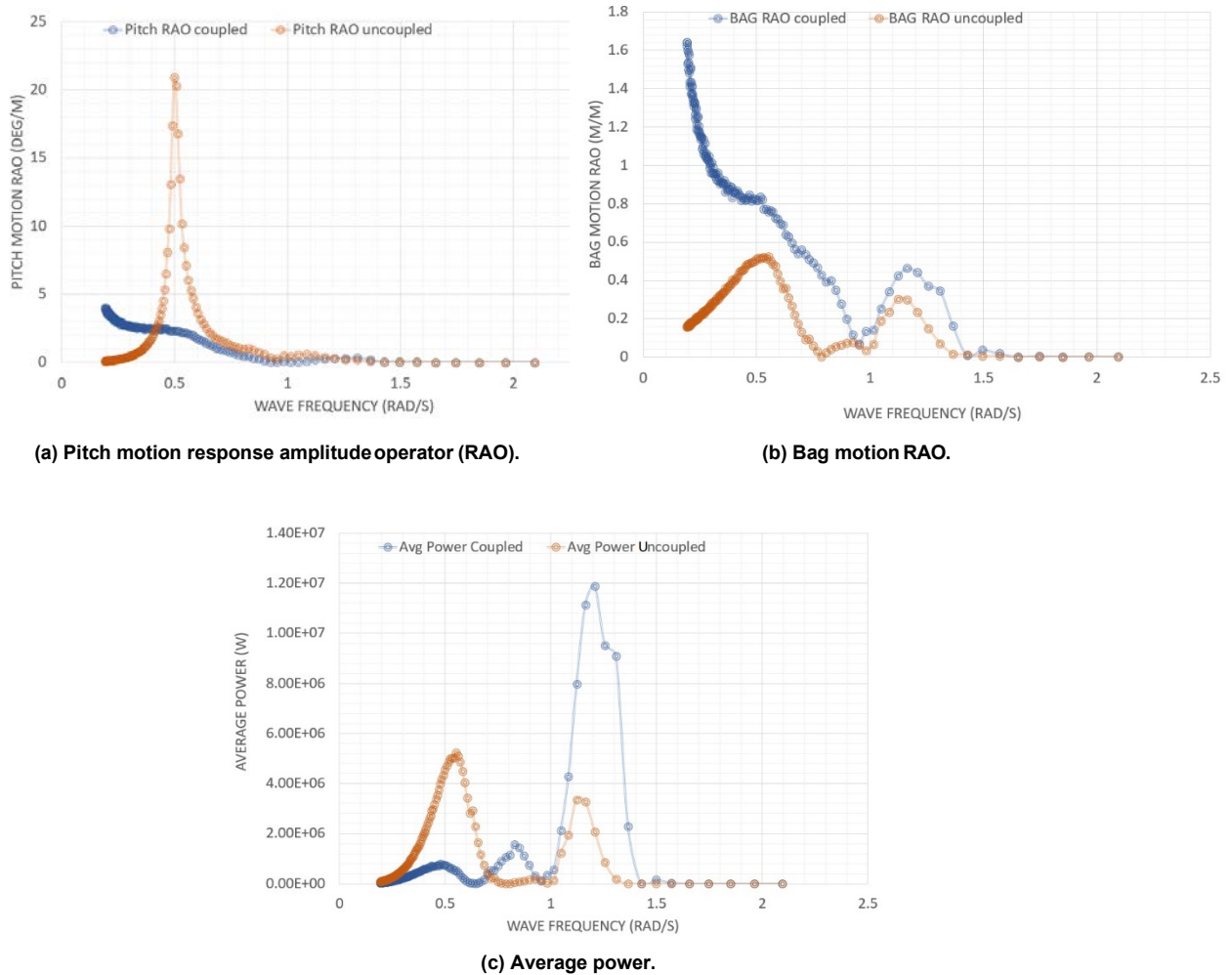


**Figure 4. Response for coupled/floating and uncoupled/fixed system.**

Fig. 4 shows the response of the numerical model with and without coupling terms. For the uncoupled model, we are only interested in the bag motion and power performance, as this configuration represents our fixed system and the pitch response of the uncoupled model is of little value in this analysis. A relatively large pitch response is evident for the coupled model for wave frequencies below 1 *rad/s*. When comparing the bag RAO (describing the piston-type bag surface displacement as illustrated in Fig. 1), a large bag response is evident for the coupled system below 1 *rad/s*. However, this large low-frequency bag response does not result in a large average power output. For lower frequencies, the coupled system produces significantly less power than the uncoupled/fixed system. The reduced power production of the coupled system for lower frequencies points to the fact that the relatively large pitch motion for lower frequencies has a negative impact on the power performance of the device.

Figure 5 illustrates different bag/pitch coupling modes. The dotted lines represent the bag position in equilibrium when the device is leveled. The bag deflection and pitch motion time series for the 12-s wave period (0.52 *rad/s*) is plotted in Fig. 6. The figure further illustrate the effect of coupling on the power production. The pitch motion of the system and the bag deflection are almost perfectly out of phase. This situation is shown in **Case B** of Fig. 5: the device experiences a positive pitch motion. The right chamber moves down and the right lower bag surface moves up. In this situation, the coupling between the bag and pitch motion reduces the pressure fluctuations in the chambers. The pitch motion by itself increases the hydrostatic and hydrodynamic pressure on the right bag surface, whereas the bag deflection counteracts this effect by moving air from the right chamber into the left chamber.

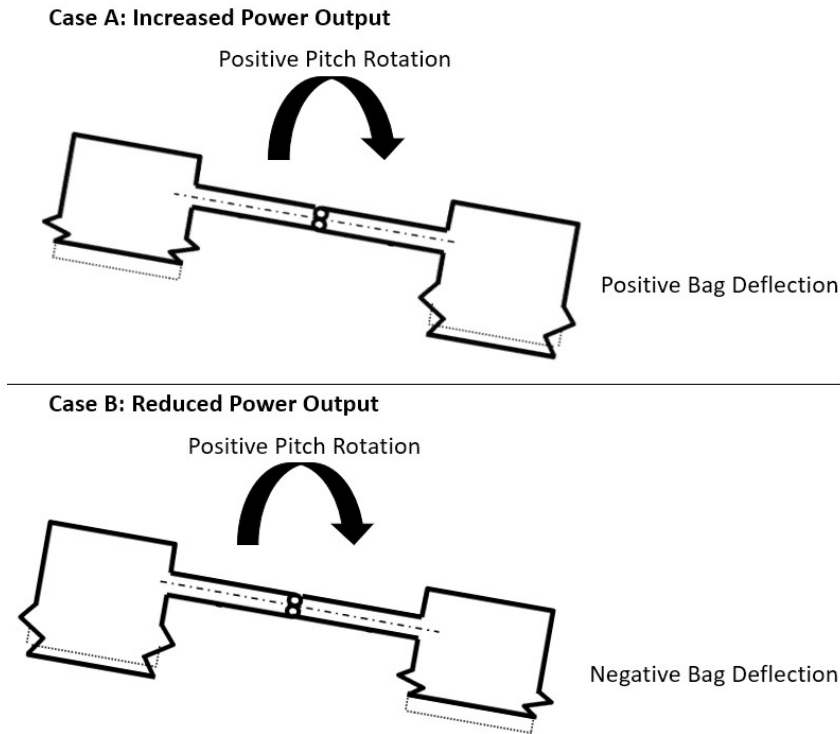


Figure 5. Illustration of different bag/pitch coupling mode.

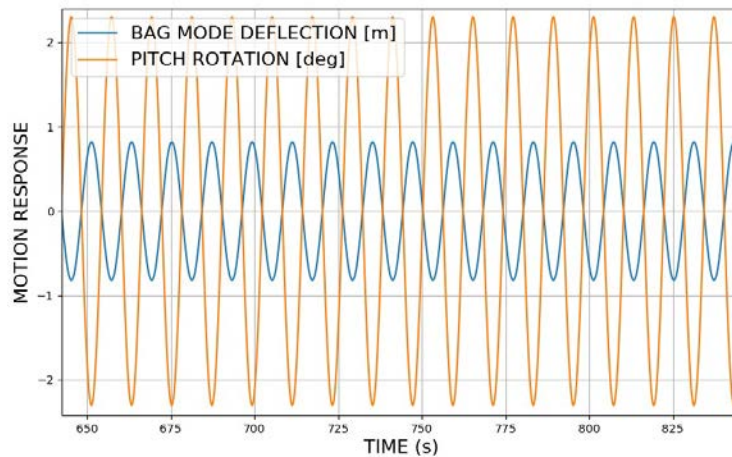


Figure 6. Bag displacement and pitch motion time series during a 12-s regular wave.

The opposite scenario can be observed for a wave period of around 5 s (**Case A** in Fig. 5). The bag and pitch motions are in phase and increase the pressure fluctuations in the chambers. The corresponding bag deflection and pitch motion time series are shown in Fig. 7. A wave period of 5 s is equivalent to about 1.26 rad/s, where a peak in average power can be observed for the coupled model in Fig. 4(c).

For both **Case A** and **Case B**, the bag motion is dominated by wave-excitation forces, while the pitch motion amplifies or decreases the pressure fluctuations in the two bags, depending on the relative phasing between the pitch and bag motion. For the current design, the coupling only has a positive impact on power performance for wave frequencies above 1 rad/s. For these higher frequencies, the waves are smaller in amplitude and carry less energy; therefore, taking advantage of this coupling effect is difficult.

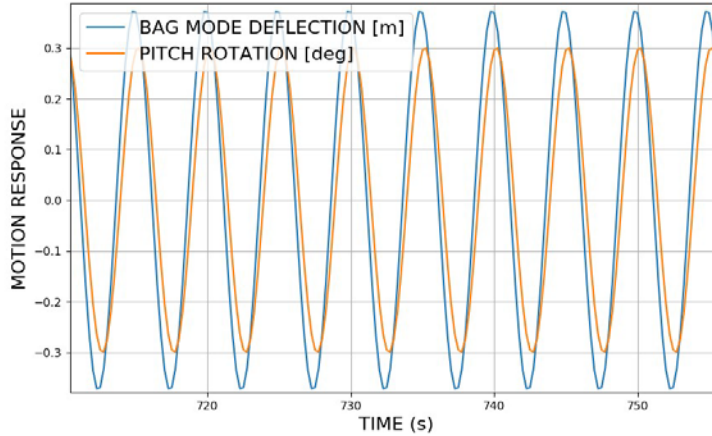


Figure 7. Bag displacement and pitch motion time series during a 5-s regular wave.

Table 1. Regular Wave Cases Used for Validation

ID	Period [s]	Freq. [rad/s]	Height [m]	$B_{PTO}$ [ $Ns/m^5$ ]
M1	6.0	1.05	0.702	15.52
M2	7.5	0.84	1.097	56.18
M3	9.0	0.70	1.580	450.64
M4	10.5	0.60	2.148	718.21
M5	12.0	0.52	2.789	727.85
M6	13.5	0.47	3.479	875.83
M7	15.0	0.42	4.188	857.81

### Comparison against Experimental Data

The validation of the numerical model is not a straightforward process, because of the relatively large uncertainty associated with the experimental data. No detailed information on the mooring system properties were available to the authors. The mooring system was represented through a linear stiffness matrix. The main diagonal entries of this matrix ( $\mathbf{K}$  in Eq. 1) were tuned to achieve a reasonable match between the motion amplitudes predicted by the numerical model and motion amplitudes recorded during the experiment for a wave period of 6 s. The regular wave cases that were used for model validation in this paper are shown in Tab. 1.

The damping coefficient that is specified to model the pressure drop over the turbine during power extraction is computed from the internal pressure and flow measurements that were collected during the experiment for each of the seven regular wave cases. As outlined in Babarit et al. 2017, the damping coefficient  $B_{PTO}$  in Eq. 2 and Eq. 3 is computed as:

$$B_{PTO} = \frac{\Delta P}{Q} \quad (4)$$

with  $\Delta P$  being the pressure drop over the turbine and  $Q$  being the flow rate through the turbine.

A comparison between the average power recorded during the experiment and the average power from the numerical simulation (coupled/floating and uncoupled/fixed model) is shown in Fig. 8. As expected from the RAO analysis, the coupled system produces more power for smaller wave periods and significantly less power than the uncoupled system for larger wave periods. Experimental power performance data and the simulated power performance of the coupled system are in relatively good agreement.

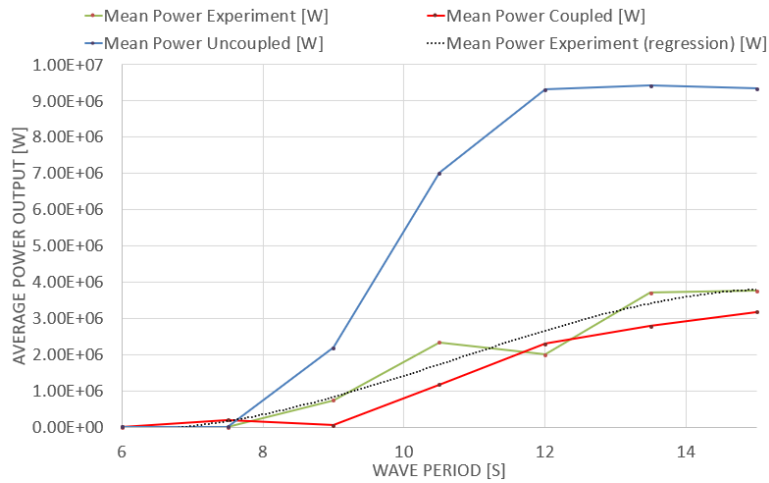


Figure 8. Average power output from experiment and simulation for different regular waves.

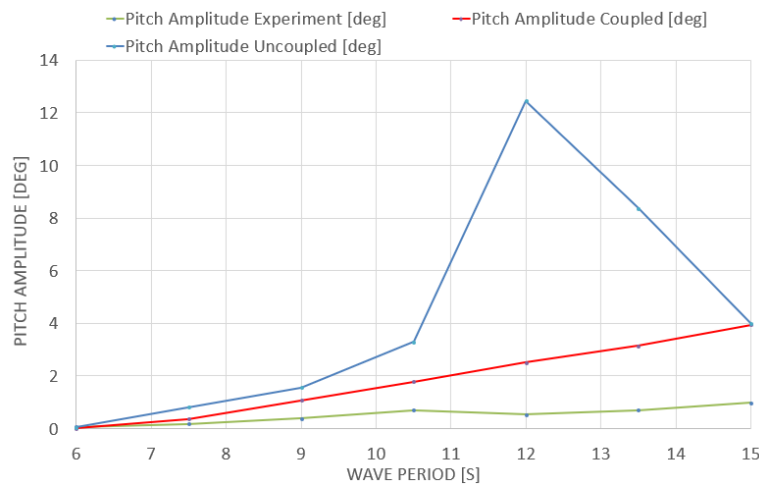
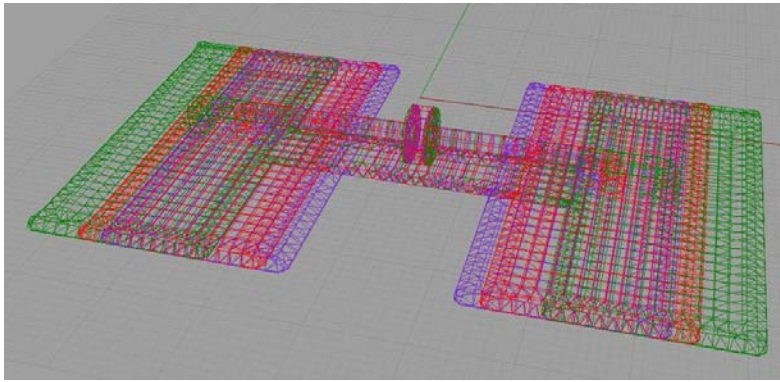


Figure 9. Pitch motion amplitude from the experiment and simulation for different regular waves.

A comparison between the pitch motion amplitude of the coupled/floating and the uncoupled/fixed numerical model and the pitch motion amplitude recorded during the experiment is shown in Fig. 9. The pitch resonance peak at about  $rad/s$  (Fig. 4 is clearly evident for the uncoupled model for wave periods of about 12 s. The overall pitch motion of the uncoupled system appears to be larger than what was recorded during the experiment. Additional tuning of the mooring stiffness matrix could help to improve the match between the simulated and experimental pitch motion amplitude. The larger pitch motion amplitude should also have a negative effect on the power production of the coupled model as discussed in the previous section. Further tuning of the mooring stiffness should therefore also decrease the differences in average power observed between the coupled model and the experimental data, as shown in Fig. 8.

## Parametric Analysis

Two different geometry variations of the original M3 model were investigated. All three models have the same bag surface area, but the length of the connecting support frame has been compressed or stretched respectively. The geometry variations are illustrated in Fig. 10. The goal here was to understand how variations in the model impact the wave frequency dependent behaviour of the system, especially in terms of power production.



**Figure 10. Illustration of investigated geometry variations (Original: Red, Longer Model: Green, Shorter Model: Blue).**

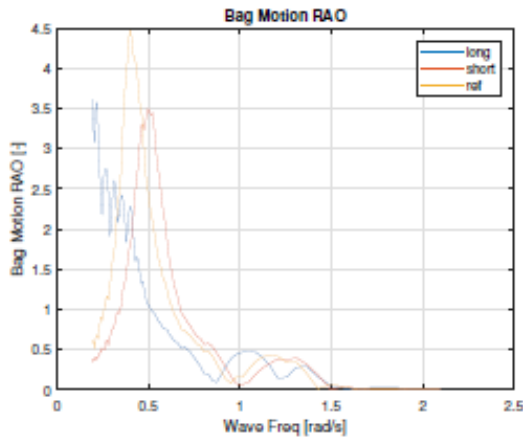
Each geometry variation was simulated in its fixed/uncoupled configuration and in its floating/coupled configuration. The frequency dependent motion response is illustrated in terms of bag motion and pitch motion RAOs for fixed and floating configurations in Fig. 11. Focusing on the two plots on the right side of Fig. 11, which represent the pitch and bag RAOs for the uncoupled configurations, one can discern that the shorter geometry (red curves) moves the RAO peaks towards higher frequencies, while the longer geometry (blue curves) moves the RAO peaks to lower frequencies. The response of the reference model with its original geometry is plotted in yellow. The behaviour described above is expected, as resonance frequency and therefore resonance wave length are directly coupled to the physical length of the device.

A similar impact of the system geometry on the motion response can be observed for the coupled model (two plots on the left side of Fig. 11). Looking at the frequency dependent power production for the fixed/uncoupled system (right plot of Fig. 12), the shorter geometry also causes the peaks for the power production to shift to higher frequencies (red curve) and the longer geometry causes a shift to lower frequencies (blue curve). As the wave energy flux scales linearly with the wave period, the longer device achieves the largest peak power compared to all three configurations. The frequency depended power production results for the floating/coupled configuration are more difficult to interpret. The second peak in the average power plot (between 1 rad/s and 1.5 rad/s) is shifted more towards higher frequencies for the shorter configuration and more towards lower frequencies for the longer configuration, which is in-line with the previous discussions, but the first peak around 0.5 rad/s is significantly smaller for the longer model. This behaviour is probably related to unfavourable coupling effects between bag and pitch motion for the longer device around 0.5 rad/s, as further discussed under "Comparison against Experimental Data".

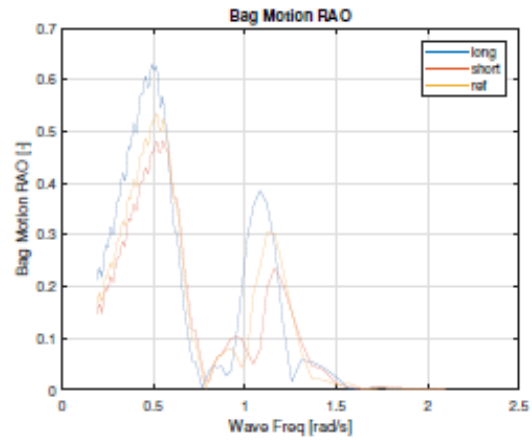
Based on these observation one can conclude that tuning the floating device to different wave conditions is not a trivial task, as a longer device not necessarily achieves a better power performance for longer, low frequency sea states, due to coupling effects between bag and pitch motion. A rigorous power performance optimization of the floating system therefore requires the utilization of a coupled model, as the one outlined within this document.

## References

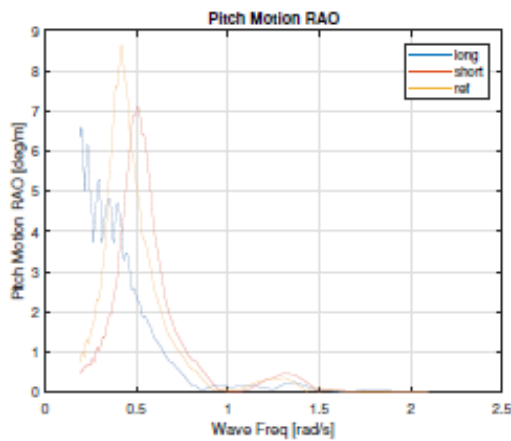
- Babarit, A., F. Wendt, Y.-H. Yu, and J. Weber. 2017. "Investigation on the energy absorption performance of a fixed-bottom pressure-differential wave energy converter." *Applied Ocean Research* 65:90–101.
- Steven, Zalek. 2016. *Test Report: Wave Energy Converter Device for M3 Wave Department of Energy Wave Energy Prize 2015*. Tech. rep. Michigan, USA: University of Michigan - Marine Hydrodynamics Laboratory - Department of Naval Architecture and Marine Engineering.
- WAMIT Inc. 2016. *WAMIT User Manual Version 7.2*. [http://www.wamit.com/manualupdate/v72\\_manual.pdf](http://www.wamit.com/manualupdate/v72_manual.pdf).
- Wendt, Fabian, Yi-hsiang Yu, and Mike Delos-reyes. 2018. "Numerical Analysis and Validation of a Pressure-Differential Wave Energy Converter." In *4th Asian Wave and Tidal Energy Conference*. Taipei, Taiwan.
- Wendt, Fabian, Amy Robertson, Jason Jonkman, and Greg Hayman. 2015. "Verification of New Floating Capabilities in FAST v8." In *AIAA SciTech 2015*. Kissimmee, FL: AIAA.
- Wendt, Fabian, Morten Andersen, Amy Robertson, and Jason Jonkman. 2016. "Verification and Validation of the New Dynamic Mooring Modules Available in FAST v8." In *26th International Ocean and Polar Engineering Conference*. Rhodes, Greece: ISOPE.



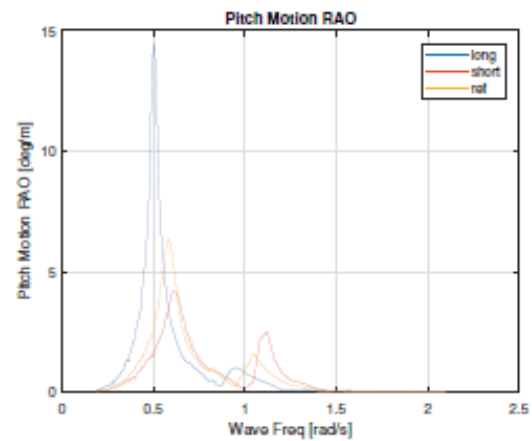
(a) Bag Motion RAO (floating system).



(b) Bag Motion RAO (fixed system).

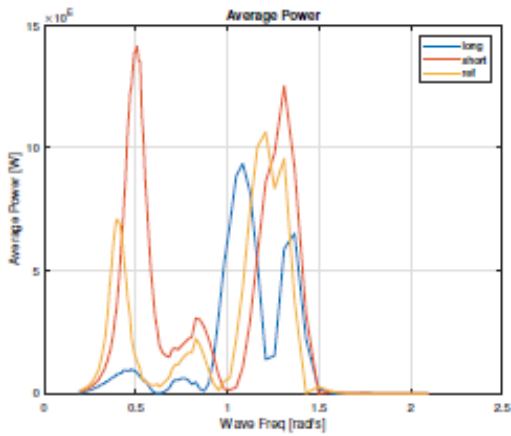


(c) Pitch Motion RAO (floating system).

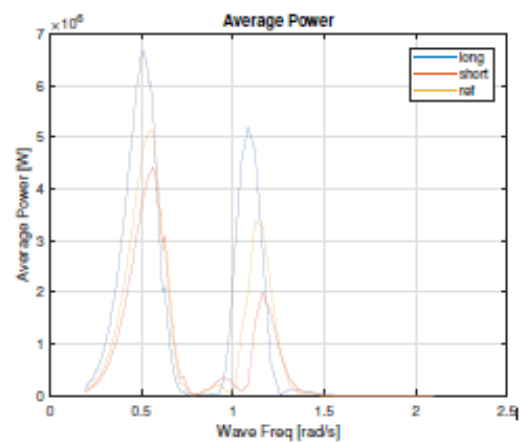


(d) Pitch Motion RAO (fixed system).

Figure 11. Motion response for different geometry variations.



(a) Bag Motion RAO (floating system).



(b) Bag Motion RAO (fixed system).

Figure 12. Motion response for different geometry variations.

# Numerical Analysis and Validation of a Pressure-Differential Wave Energy Converter

Fabian Wendt\*, Yi-Hsiang Yu\*, Aurélien Babarit<sup>†</sup>, Mike Delos-Reyes<sup>‡</sup>

\*National Renewable Energy Laboratory (NREL) Golden, Colorado 80401, USA

E-mail: fabian.wendt@nrel.gov, yi-hsiang.yu@nrel.gov

<sup>†</sup>EC Nantes, LHEEA Lab.

Nantes, France

E-mail: aurelien.babarit@ec-nantes.fr

<sup>‡</sup>M3 WAVE

Corvallis, OR, USA

E-mail: info@m3wave.com

**Abstract**—A pressure-differential wave energy converter (WEC) is a unique design, compared to conventional kinematic WECs. It contains two flexible, air-filled bags that turn pressure fluctuations caused by ocean waves and swells into alternating expansion and compression cycles. The two bags are strategically oriented based on the dominant wave environment and exchange air back and forth with each passing wave. A turbine is located between the two bags and used to extract power from the internal airflow.

A fixed-bottom pressure-differential design can be directly analyzed in the frequency domain by modeling the bag motion as a generalized body mode. However, for a floating system, the device motion influences its power output and a coupled analysis approach is required. As a result, the authors developed a time-domain numerical model to analyze the floating pressure-differential WEC system.

The equations of motion describing the bag and rigid body motion of the device are solved in a coupled fashion. The hydrodynamic diffraction and radiation coefficients for all relevant system motions have been computed via WAMIT. The bag motion was introduced within WAMIT as an additional generalized body mode. The hydrodynamic performance of the system is validated against 1:50-scale wave tank measurements and the influence of motion coupling on the power performance is characterized.

**Index Terms**—wave energy, pressure differential, generalized modes, WAMIT, M3

## I. INTRODUCTION

Numerous studies have shown that extracting energy from ocean wave resources has the potential to provide a significant contribution to the electricity supply [1]. In the past several decades, a wide variety of wave energy converter (WEC) technologies has been proposed, including oscillating water columns, oscillating body type designs, and over-topping devices [2]. However, wave energy technology is still in the research and development stage. Therefore, levelized cost of energy (LCOE) for WEC designs is still high, compared to other renewable energy technologies, such as wind and solar [3].

Although the cost may gradually decrease with industrialization and mass production as large WEC farms are being developed, it is essential to find an efficient pathway to reduce that cost for the WEC industry to be successful. Several innovative WEC technologies have been proposed recently, including the use of flexible material that will minimize the load on the device and reduce the overall LCOE [4]–[6]. This work is focused on pressure-differential wave energy conversion, which is a unique approach compared to conventional kinematic WECs. Pressure-differential WECs contain two (or more) air-filled bags

that turn ocean-wave-induced pressure fluctuations into alternating expansion and compression cycles, as shown in Fig. 1. The two bags are strategically oriented based on the dominant wave environment and exchange air back and forth with each passing wave. A study on a bottom-fixed pressure-differential WEC was conducted by Babarit et al. [4], which indicated that the pressure-differential WEC could be highly efficient both with respect to energy absorption and economic potential.

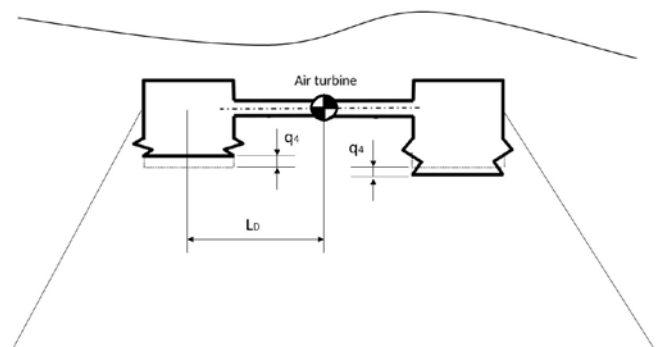


Fig. 1. A taut moored M3 device with a piston-type bag mode shape. Graphic based on [4].

## II. NUMERICAL MODEL

A numerical model was developed to simulate the taut moored M3 device for regular wave conditions. M3 Wave LLC is a company out of Oregon that has been developing the pressure-differential wave energy technology since the early 1990s [7].

In this work, the numerical model was solved in the time domain to account for quadratic damping components. The convolution integral that is typically used in Cummins-type time domain models [8] was not implemented, because of the fact that only regular wave cases were investigated and no significant nonlinear behaviour of the model was to be expected. The bag displacement is modeled as a piston type motion (Fig. 1). The utilized equations of motion are based on the work presented in [4], but additional degrees of freedom have been introduced to account for the motion of the device in its moored configuration. Compared to [4], an additional constraint has been formulated by modeling the bag motion as a single mode shape (e.g., the left bag moves down and the right bag moves up). This additional constraint was introduced to further simplify the equations of motion. Due to the fact that only one wave direction was considered here, only the surge (1), heave (2), pitch (3), and

bag motion (4) degrees of freedom were included in the numerical model. The equations of motion used in the numerical model are outlined below. They are formulated at the center of gravity which is located at the geometric center of the device (see Fig 1).

$$\mathbf{A}\ddot{\mathbf{q}} + \mathbf{B}\dot{\mathbf{q}} + \mathbf{D}\mathbf{v} + 0.5\mathbf{S}(\mathbf{p}_1 + \mathbf{p}_2) + (\mathbf{K} + \mathbf{C})\mathbf{q} = \mathbf{F}_{\text{ex}} \quad (1)$$

$$\dot{p}_1 - 0.5 \frac{p_s}{v_s} \mathbf{R}\dot{\mathbf{q}} + \frac{p_s}{v_s} \frac{p_1}{B_{PTO}} - \frac{p_s}{v_s} \frac{p_2}{B_{PTO}} = 0 \quad (2)$$

$$\dot{p}_2 + 0.5 \frac{p_s}{v_s} \mathbf{R}\dot{\mathbf{q}} - \frac{p_s}{v_s} \frac{p_1}{B_{PTO}} + \frac{p_s}{v_s} \frac{p_2}{B_{PTO}} = 0 \quad (3)$$

The matrix  $\mathbf{S}$  is only populated along the main diagonal and describes the relevant surface area that is participating in coupled motion response between the rigid body modes and bag motion (Eq. 4)

$$\mathbf{S}_{ii} = \int \int_{A_i} m_4 w_i dS \quad i = \{1..4\} \quad (4)$$

$$m_j = \mathbf{M}_j(\mathbf{x}) \cdot \mathbf{n}_g \quad j = \{1..4\} \quad (5)$$

$$\mathbf{C}_{ij} = d_{ij} \int \int_{A_j} m_j w_i dS \quad i, j = \{1..4\} \quad (6)$$

$$d_{ij} = \rho g \quad \forall \{i < 4 \wedge j < 4\} \quad (7)$$

$$d_{ij} = (\rho - \rho')g \quad \forall \{i > 3 \vee j > 3\} \quad (8)$$

With  $m_j$  being the normal component of the  $j$ th mode shape relative to the body surface and  $w_i$  being the vertical component of the displacement vector of the  $i$ th mode.

The scalar value,  $m_j$ , is being computed as the dot product of the local mode shape displacement vector,  $\mathbf{M}_j(\mathbf{x})$ , at the location  $\mathbf{x}$  on the body surface, and the normal vector,  $\mathbf{n}_g$ , that points from the wetted surface participating in the  $j$ th mode shape, ( $A_j$ ), into the body. The 4x1 vector,  $\mathbf{q}$ , and its derivatives describe the motion of the system (displacement, velocity, and acceleration) of the four degrees of freedom present in the system (three rigid body modes and one generalized mode).

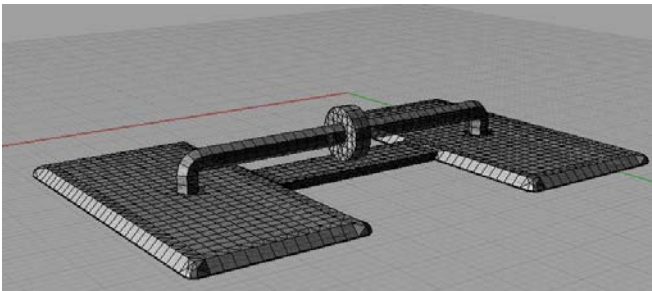


Fig. 2. Top isometric view of the WAMIT mesh.

The 1x4 row vector,  $\mathbf{R}$ , contains the same entries as the diagonal of the  $\mathbf{S}$  matrix, arranged in a single row, and describes how the bag deforms as a result of coupled motion.

The  $\mathbf{p}_1$  and  $\mathbf{p}_2$  vectors are simply populated with the  $\rho_1$  and  $\rho_2$  values:  $\mathbf{p}_{1_i} = \rho_1$  and  $\mathbf{p}_{2_i} = \rho_2$  for  $i = 1$  to 4.

The  $\mathbf{A}$  matrix contains mass and inertia contributions from the device itself and from added mass effects.  $\mathbf{B}$  is the linear radiation damping matrix. Frequency-dependent added mass and radiation damping are computed via WAMIT.

The  $\mathbf{K}$  matrix represents the linear restoring contribution from the mooring system and the  $\mathbf{C}$  matrix contains the hydrostatic stiffness terms as described in Eq. 6.

Quadratic damping resulting from viscous effects is included in the equation of motion through the  $\mathbf{D}$  matrix and the  $\mathbf{v}$  vector as outlined in Eq. 9 and Eq. 10. A value of 8.0 was

assigned to the viscous drag coefficient,  $C_d$ . Drag coefficients in the range between 8 and 10 are oftentimes used to model the viscous effects in heave plates for offshore structures [9], [10].

$$\mathbf{D} = \begin{bmatrix} 0 & 0 & 0 & 0 \\ 0 & \mathbf{S}_{4,4}C_d & 0 & 0 \\ 0 & 0 & \frac{1}{2L_D}\mathbf{S}_{3,3}C_d & \frac{1}{2L_D}\mathbf{S}_{3,4}C_d \\ 0 & 0 & \frac{1}{2L_D}\mathbf{S}_{3,4}C_d & \mathbf{S}_{4,4}C_d \end{bmatrix} \quad (9)$$

$$\mathbf{v} = \begin{bmatrix} \dot{q}_1^2 \\ \dot{q}_2^2 \\ (\dot{q}_3 L_D)^2 \\ \dot{q}_4^2 \end{bmatrix} \quad (10)$$

The water density, ( $1025 \frac{\text{kg}}{\text{m}^3}$ ), is given as  $\rho$ , while  $\rho'$  describes the density of the working fluid inside the wave energy device (in this case, air with  $1.225 \frac{\text{kg}}{\text{m}^3}$ ). The equations of motion (Eq. 1–Eq. 3) can be formulated as a system of differential equations and solved numerically. The linear damping, added mass, and wave-excitation loads ( $\mathbf{F}_{\text{ex}}$ ) caused by Froude-Krylov and scattering forces were computed via WAMIT [11]. An illustration of the utilized WAMIT mesh is shown in Fig. 2 and Fig. 3. The bag area that is participating in the piston motion is highlighted in orange.

### III. WAVE TANK TESTING

A 1:50-scale version of the taut moored M3 device has been tested in the tow tank of the Marine Hydrodynamics Laboratory at the University of Michigan during the U.S. Department of Energy Wave Energy Prize in January 2016 [12]. The goal of the tests was the experimental characterization of the system's power performance over a range of different wave conditions. The M3 device uses a turbine in the middle of the tube that connects the two flexible chambers to generate electrical power. For the model-scale test, the turbine was modeled through a simple orifice plate. The plate geometry was selected so that it produces a pressure drop similar to what would be expected from a model-scale turbine. Photos of the tow tank and the M3 device installed in the tow tank are shown in Fig. 4 and Fig. 5, respectively.

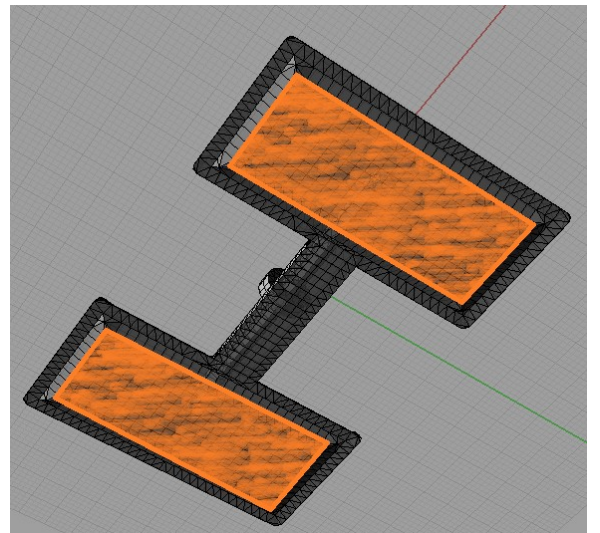


Fig. 3. Bottom isometric view of the WAMIT mesh; the bag surface participating in the piston mode shape is highlighted in orange.



Fig. 4. Marine Hydrodynamics Laboratory tow tank and carriage [12].



Fig. 5. Scaled M3 device installed in the tow tank [12].

During the test, the generated power was computed from the measured pressure drop over the orifice plate. The exact procedure that was used to transfer the pressure measurements into an estimate of the generated power was not available to the authors. The device motions were recorded through an optical measurement system. The exact position relative to the device center that was used to report these motions was not known to the authors. Because of the large uncertainties associated with the recorded time series data, the authors focused their validation efforts on the motion amplitude and average power production data that were reported in table format for each test case.

#### IV. COMPARISON OF FIXED VERSUS FLOATING SYSTEM

To characterize the dynamic response of the numerical model, we computed the response amplitude operators (RAOs) and the averaged power production over a large range of different regular wave periods. Comparing a fixed versus a moored/floating configuration was one important aspect of our analysis. In the numerical model, the fixed configuration was realized by removing all coupling terms from the equations of motion (Eq. 1–Eq. 3). This approach yields a system of equations in which each degree of freedom is solved independently and the power performance and bag motion will not be impacted by the motion of the device (which basically represents a fixed system). Comparing the coupled and uncoupled numerical model makes it possible to quantify the impact of the device motion on the power performance of the system. All results presented and discussed in this paper are referring to the full scale version of the system. The length from chamber to device center ( $LD$  in Fig. 1) for the full scale system is 25.0 m. The bottom of the device is submerged 12 m below the free surface.

Fig. 6 shows the pitch RAO of the numerical model with and without coupling terms. For the uncoupled model, we are only interested in the bag motion and power performance, as this configuration represents our fixed system and the pitch response of the uncoupled model is of little value in this analysis. A relatively large pitch response is evident for the coupled model for wave frequencies below 1  $rad/s$ . When comparing the bag RAO (describing the piston-type bag surface displacement as illustrated in Fig. 1), a large bag response is evident for the coupled system below 1  $rad/s$  (Fig. 7). However, this large low-frequency bag response does not result in a large average power output. For lower frequencies, the coupled system produces significantly less power than the uncoupled/fixed system (Fig. 8). The reduced power production of the coupled system for lower frequencies points to the fact that the relatively large pitch motion for lower frequencies has a negative impact on the power performance of the device.

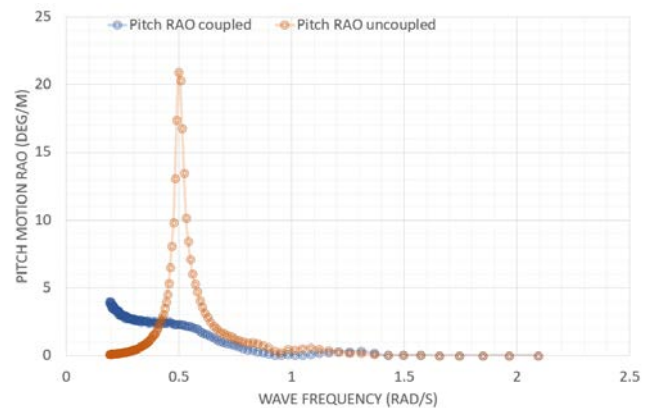


Fig. 6. Coupled/floating and uncoupled/fixed pitch motion response amplitude operator (RAO).

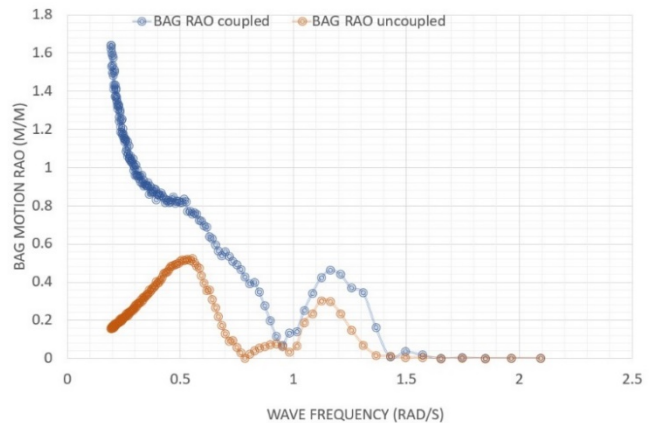


Fig. 7. Coupled/floating and uncoupled/fixed bag motion RAO.

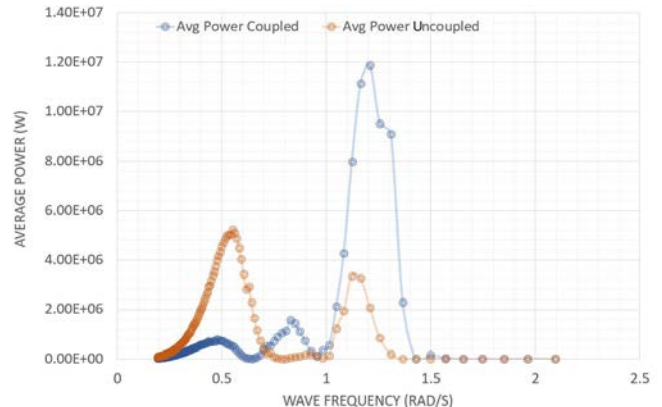


Fig. 8. Average power for coupled/floating and uncoupled/fixed system.

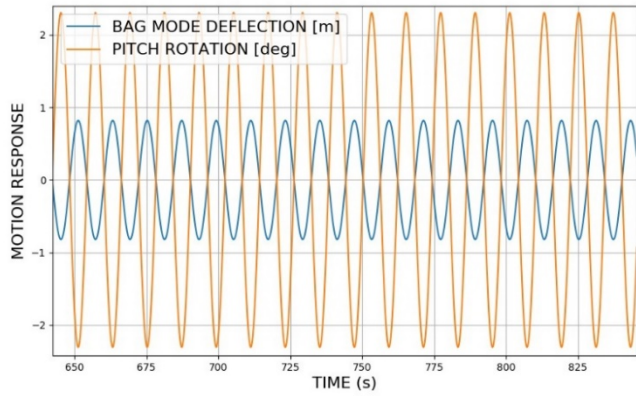


Fig. 9. Bag displacement and pitch motion time series during a 12-s regular wave.

The bag deflection and pitch motion time series plots for the 12-s wave period ( $0.52 \text{ rad/s}$ ) further illustrate the effect of coupling on the power production (Fig. 9). The pitch motion of the system and the bag deflection are almost perfectly out of phase.

This situation is shown in **Case B** of Fig. 10: the device experiences a positive pitch motion. The right chamber moves down and the right lower bag surface moves up. In this situation, the coupling between the bag and pitch motion reduces the pressure fluctuations in the chambers. The pitch motion by itself increases the hydrostatic and hydrodynamic pressure on the right bag surface, whereas the bag deflection counteracts this effect by moving air from the right chamber into the left chamber.

The opposite scenario can be observed for a wave period of around 5 s (**Case A** in Fig. 10). The bag and pitch motions are in phase and increase the pressure fluctuations in the chambers. The corresponding bag deflection and pitch motion time series are shown in Fig. 11. A wave period of 5 s is equivalent to about  $1.26 \text{ rad/s}$ , where a peak in average power can be observed for the coupled model in Fig. 8. For both **Case A** and **Case B**, the bag motion is dominated by wave-excitation forces, while the pitch motion amplifies or decreases the pressure fluctuations in the two bags, depending on the relative phasing between the pitch and bag motion.

For the current design, the coupling only has a positive impact on power performance for wave frequencies above  $1 \text{ rad/s}$ . For these higher frequencies, the waves are smaller in amplitude and carry less energy; therefore, taking advantage of this coupling effect is difficult.

## V. COMPARISON AGAINST EXPERIMENTAL DATA

The validation of the numerical model is not a straightforward process, because of the relatively large uncertainty associated with the experimental data. No detailed information on the mooring system properties were available to the authors. The mooring system was represented through a linear stiffness matrix. The main diagonal entries of this matrix ( $\mathbf{K}$  in Eq. were tuned to achieve a reasonable match between the motion amplitudes predicted by the numerical model and motion amplitudes recorded during the experiment for a wave period of 6 s. The regular wave cases that were used for model validation in this paper are shown in Tab. I.

TABLE I  
REGULAR WAVE CASES USED FOR VALIDATION

ID	Period [s]	Freq. [rad/s]	Height [m]	$B_{PTO}$ [ $\frac{N \cdot s}{m^3}$ ]
M1	6.0	1.05	0.702	15.52
M2	7.5	0.84	1.097	56.18
M3	9.0	0.70	1.580	450.64
M4	10.5	0.60	2.148	718.21
M5	12.0	0.52	2.789	727.85
M6	13.5	0.47	3.479	875.83
M7	15.0	0.42	4.188	857.81

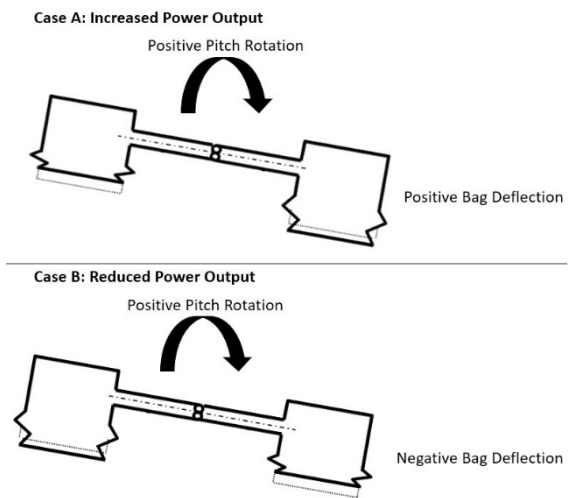


Fig. 10. Illustration of different bag/pitch coupling modi. The dotted lines represent the bag position in equilibrium when the device is leveled.

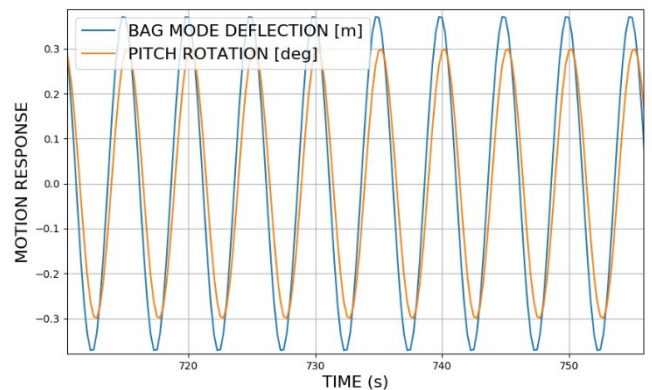


Fig. 11. Bag displacement and pitch motion time series during a 5-s regular wave.

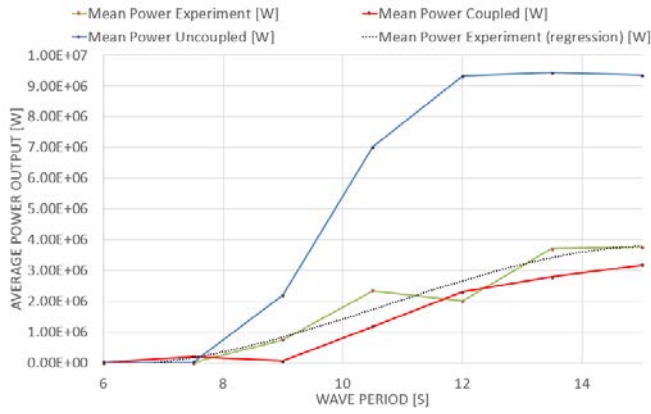


Fig. 12. Average power output from experiment and simulation for different regular waves.

The damping coefficient that is specified to model the pressure drop over the turbine during power extraction is computed from the internal pressure and flow measurements that were collected during the experiment for each of these seven regular wave cases. As outlined in [4], the damping coefficient  $B_{PTO}$  in Eq. 2 and Eq. 3 is computed as:

$$B_{PTO} = \frac{\Delta P}{Q} \quad (11)$$

with  $\Delta P$  being the pressure drop over the turbine and  $Q$  being the flow rate through the turbine.

A comparison between the average power recorded during the experiment and the average power from the numerical simulation (coupled/floating and uncoupled/fixed model) is shown in Fig. 12. As expected from the RAO analysis, the coupled system produces more power for smaller wave periods and significantly less power than the uncoupled system for larger wave periods. Experimental power performance data and the simulated power performance of the coupled system are in relatively good agreement.

A comparison between the pitch motion amplitude of the coupled/floating and the uncoupled/fixed numerical model and the pitch motion amplitude recorded during the experiment is shown in Fig. 13.

The pitch resonance peak at about 0.5 *rad/s* (Fig. 6 is clearly evident for the uncoupled model for wave periods of about 12 s. The overall pitch motion of the uncoupled system appears to be larger than what was recorded during the experiment. Additional tuning of the mooring stiffness matrix could help to improve the match between the simulated and experimental pitch motion amplitude. The larger pitch motion amplitude should also have a negative effect on the power production of the coupled model as discussed in the previous section. Further tuning of the mooring stiffness should therefore also decrease the differences in average power observed between the coupled model and the experimental data, as shown in Fig. 12.

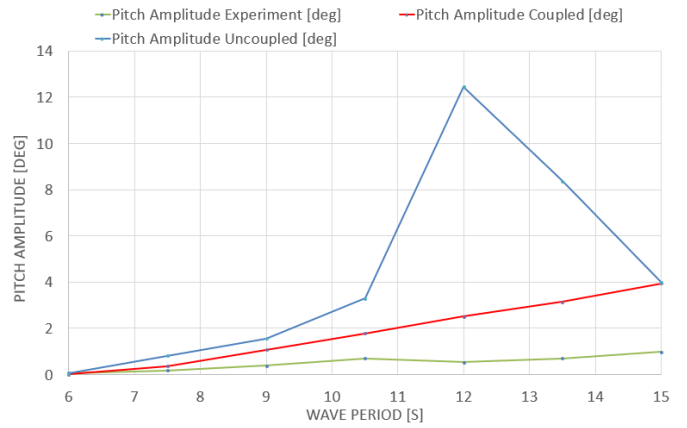


Fig. 13. Pitch motion amplitude from the experiment and simulation for different regular waves.

## VI. CONCLUSION

A scaled version of the M3 device has been tested in a floating/moored configuration at the Marine Hydrodynamics Laboratory (University of Michigan) during the U.S. Department of Energy Wave Energy Prize in 2016. The device motion and power performance were recorded during the test campaign. Based on the equations introduced in [4], the authors developed a numerical model to simulate the M3 device as a floating and a fixed system. To study the power performance of the fixed numerical model, all coupling terms were simply set to zero. Given the larger uncertainty associated with the experimental data, relatively good agreement was found in terms of pitch motion and power performance between the experimental data and the floating/coupled numerical model. Coupling between the pitch and bag motion was found to have positive effects on power production for certain wave frequency regions. The relative phase between pitch motion response and the bag displacement is a key factor regarding the power performance of the floating device.

## ACKNOWLEDGMENT

The Alliance for Sustainable Energy, LLC, (Alliance) is the manager and operator of the National Renewable Energy Laboratory (NREL). NREL is a national laboratory of the U.S. Department of Energy, Office of Energy Efficiency and Renewable Energy. This work was authored by the Alliance and supported by the U.S. Department of Energy under Contract No. DE-AC36-08GO28308. Funding was provided by the U.S. Department of Energy Office of Energy Efficiency and Renewable Energy, Water Power Technologies Office. The views expressed in the article do not necessarily represent the views of the U.S. Department of Energy or the U.S. government. The U.S. government retains, and the publisher, by accepting the document for publication, acknowledges that the U.S. government retains a nonexclusive, paid-up, irrevocable, worldwide license to publish or reproduce the published form of this work, or allow others to do so, for U.S. government purposes.

## REFERENCES

- [1] K. Gunn and C. Stock-Williams, "Quantifying the global wave power resource," *Renewable Energy*, vol. 44, pp. 296–304, 2012.
- [2] A. F. D. O. Falcao, "Wave Energy Utilization: A Review of the Technologies," *Renewable and Sustainable Energy Reviews*, vol. 14, pp. 899–918, 2010.
- [3] D. S. Jenne, Y.-H. Yu, and V. Neary, "Levelized Cost of Energy Analysis of Marine and Hydrokinetic Reference Models," in *3rd Marine Energy Technology Symposium*. Washington, DC, United States: METS, 2015.
- [4] A. Babarit, F. Wendt, Y.-H. Yu, and J. Weber, "Investigation on the energy absorption performance of a fixed-bottom pressure-differential wave energy converter," *Applied Ocean Research*, vol. 65, pp. 90–101, 2017.
- [5] "SBM Offshore." [Online]. Available: <https://www.sbmoffshore.com/what-we-do/our-products/renewables/>
- [6] J. C. McNatt, H. T. Ozkan-Haller, M. Morrow, and M. Delos-Reyes, "Preliminary Modeling and Analysis of a Horizontal Pressure Differential Wave Energy Converter," *Journal of Offshore Mechanics and Arctic Engineering*, vol. 136, no. 1, p. 011901, 2013. [Online]. Available: <http://offshoremechanics.asmedigitalcollection.asme.org/article.aspx?doi=10.1115/1.4025437>
- [7] M3 Wave LLC, "M3 wave," <https://www.m3wave.com/>, 2014.
- [8] W. Cummins, "The Impulse Response Function and Ship Motions," David Taylor Model Basin (DTNSRDC), Tech. Rep., 1962.
- [9] F. Wendt, M. Andersen, A. Robertson, and J. Jonkman, "Verification and Validation of the New Dynamic Mooring Modules Available in FAST v8," in *26th International Ocean and Polar Engineering Conference*. Rhodes, Greece: ISOPE, 2016.
- [10] F. Wendt, A. Robertson, J. Jonkman, and G. Hayman, "Verification of New Floating Capabilities in FAST v8," in AIAA SciTech 2015. Kissimmee, FL: IAA, 2015.
- [11] WAMIT Inc., "Wamit user manual version 7.2," [http://www.wamit.com/manualupdate/v72 manual.pdf](http://www.wamit.com/manualupdate/v72%20manual.pdf), 2016.
- [12] Z. Steven, "Test Report: Wave Energy Converter Device for M3 Wave Department of Energy Wave Energy Prize 2015," University of Michigan - Marine Hydrodynamics Laboratory - Department of Naval Architecture and Marine Engineering, Michigan, USA, Tech. Rep., 2016.